J. Fluid Mech. (1982), *vol.* 125, *pp.* 429–451
Printed in Great Britain

Free convection in vertical gaps

By J. N. KOSTER AND U. MÜLLER
Kernforschungszentrum Karlsruhe, Institut für Reaktorbauelemente, Postfach 3640, 7500 Karlsruhe 1, Federal Republic of Germany

(Received 16 April 1981 and in revised form 3 May 1982)

Free convective flow was investigated experimentally in a variety of slender vertical gaps of large horizontal extent. Temperature fields were visualized by holographic real-time interferometry, and local temperatures measured by thermocouples at the lower and upper boundaries of the gap as well as in the fluid. The critical Rayleigh number at the onset of convection was determined for different gap geometries (aspect ratios) and different thermal properties of the sidewalls and the fluid. For supercritical Rayleigh numbers, bounds of stability of steady-state two-dimensional convection were determined for transient and oscillatory states of the flow. The oscillatory flow is caused by an instability of the thermal boundary layers at the lower and upper boundaries, as evidenced by direct interferometric observation and by the measured period of oscillation depending on the Rayleigh number. The oscillations of the flow exhibit a periodic behaviour at the threshold from steady to unsteady flow. However, the periodic character of the oscillations is superseded by stochastic features immediately beyond the threshold Rayleigh number.

1. Introduction

Since the study of Wooding (1960) free convective flow in slender vertical gaps, where one horizontal dimension is much smaller than the other, has been investigated in order to simulate convective flow through porous media.

In a fluid-saturated porous medium low-Reynolds-number flow of an incompressible fluid is described by a linear pressure–velocity relation, called Darcy's law (Darcy 1856):

$$\mathbf{v} = -\frac{K}{\mu}(\nabla p - \rho \mathbf{g}), \tag{1}$$

where $\mathbf{v}$ is the filtration velocity vector, ∇p the pressure gradient, ρ the density, μ the dynamic viscosity, K the permeability of the medium and g the acceleration due to gravity. Hele-Shaw (1898) developed an analogy between an isothermal two-dimensional flow in a porous medium and the motion of an isothermal fluid between two parallel plates separated by a distance d. The mean velocity for the flow through a so-called Hele-Shaw cell is thus

$$\mathbf{v} = -\frac{d^2}{12\mu}(\nabla p - \rho \mathbf{g}) \tag{2}$$

(Lamb 1975). The hydraulic analogy between viscous fluid motion in a porous medium and motion in a Hele-Shaw cell is rigorous for isothermal flow when an equivalent permeability $K = \frac{1}{12}d^2$ is defined. The Hele-Shaw cell thus enables the experimentalist to simulate the flow through a porous medium (Bear 1972).

However, when there are temperature variations in the liquid–solid system of the

porous medium the thermal interaction between the liquid and the solid surface is generally difficult to model. Therefore, schemes of averaging the thermal properties for the whole system were employed in the past in order to establish analytically treatable models. It has been suggested that convection in Hele-Shaw cells could be characterized by a single properly defined Rayleigh number. In analogy to convection in porous media, such a Rayleigh number is defined as

$$Ra^{\mathrm{HS}} = \beta g \Delta T h K (\nu \kappa_{\mathrm{m}})^{-1}, \tag{3}$$

where β is the coefficient of thermal expansion, ΔT the temperature difference between bottom and top of the gap, h the height of the cell, ν the kinematic viscosity and κ_{m} an average combined thermal diffusivity of the fluid and the solid sidewalls.

Elder (1967*a*), Horne & O'Sullivan (1974, 1978) and Hartline & Lister (1977) each adopted different combinations of definitions for the permeability K and the average thermal diffusivity κ_{m}.

Elder (1967*a*,*b*, 1968) gave a detailed theoretical analysis of various flow phenomena, which he also observed experimentally. Describing his results, Elder employed the average thermal diffusivity $\kappa_{\mathrm{m}} = k_{\mathrm{m}}(\rho c)_{\mathrm{f}}^{-1}$, where k_{m} is the thermal conductivity of the saturated medium and $(\rho c)_{\mathrm{f}}$ is the thermal capacity of the fluid, and the permeability $K = \frac{1}{12}d^2$. Recently, Hartline & Lister (1977, 1978) carried out careful measurements of the critical Rayleigh number and the flow velocity of thermal convection in Hele-Shaw cells under supercritical conditions. They utilized the relation $\kappa_{\mathrm{m}} = (k_{\mathrm{f}}\epsilon + k_{\mathrm{s}}(1-\epsilon))/(\rho c)_{\mathrm{f}}$, where k_{f} and k_{s} are the thermal conductivities of the fluid and solid respectively, $\epsilon = d/Y$ and $K = \frac{1}{12}\epsilon d^2 = d^3/12Y$, where Y is the width of the Hele-Shaw cell (see figure 1).

All the aforementioned authors claim that their experimental results (e.g. the onset of convection) are in reasonable agreement with the theoretical predictions of Lapwood (1948). According to his theory for a horizontal, infinitely wide, saturated porous layer between two horizontal impervious walls, convection starts at a critical Rayleigh number $Ra_{\mathrm{c}}^{\mathrm{HS}} = 4\pi^2$. However, when we tried to confirm the predictions of Lapwood and the aforementioned experimental results we found agreement or disagreement depending on the different combinations of wall material and fluid that we chose for the design of our Hele-Shaw cells. In order to clarify this phenomenon, further experimental investigations were carried out. In this study the Rayleigh number used is defined in the following way:

$$Ra = \beta g \Delta T h^3 (\kappa_{\mathrm{f}} \nu_{\mathrm{f}})^{-1}, \tag{4}$$

where the fluid properties are indicated by the subscript f. This definition corresponds to that in the classical Bénard problem (Bénard 1900) of an infinitely extended horizontal fluid layer that is heated from below. The aspect ratio $A = h/d$ (see figure 1) is considered as a parameter. The results of our investigations are compared subsequently with recent theoretical findings obtained by other researchers (Kvernvold 1979; Frick & Clever 1980, 1982; Frick 1981).

Recent developments in convective-flow research have shown that several distinct phenomena occur during the transition from steady-state to time-dependent stochastic convective flow. The time-dependent flows often show a periodic character at first. But at higher Rayleigh numbers the flow may become quasi-periodic, followed by a stochastic behaviour, depending on the aspect ratios of the test volume. Investigations dealing with time-dependent flow in boxes of aspect ratios of around unity were reported by, for example, Ahlers & Behringer (1978*a*, *b*), Gollub & Benson (1978, 1980) and Dubois & Bergé (1981). Time-dependent convective flows in

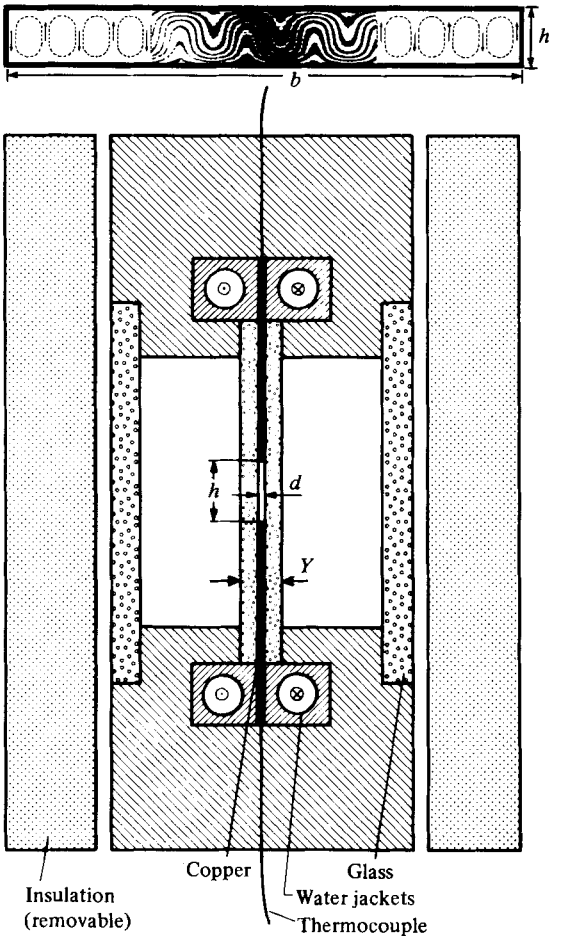

FIGURE 1. Cross-section of the Hele-Shaw cell and a typical interferogram of a Plexiglas-bounded cell illustrating the temperature field and corresponding streamlines of the flow. h is the height of the fluid-filled gap; d is the depth; b is the length; Y is the thickness of the cell. Aspect ratios: $h/d \gg 1$ and $h/b \ll 1$.

Hele-Shaw cells were considered theoretically by Kvernvold (1979) and Frick (1981). So far, however, no Hele-Shaw-cell experiments have been reported that give support to the theories of time-dependent convective flows.

The experimental results reported here concern mainly three topics. The onset of convection is discussed in §3, the stability of two-dimensional convection in §4, and the spatial and temporal structures of the time-dependent convective flow in §5.

2. Experimental set-up and procedures

Experiments were performed in various Hele-Shaw cells of common length $b = 430$ mm, variable height $18 < h/\text{mm} < 60$ and variable gap width $1 < d/\text{mm} < 3$. A schematic sketch of such a cell is shown in figure 1. The Hele-Shaw cells were designed for the investigation of convective flow by interferometric techniques. The transparent sidewalls were made out of glass or Plexiglas of

different thicknesses. The gap width d plus the thickness of the two walls is called Y, as in Hartline & Lister (1977). Copper shims clamped between the transparent sidewalls formed the horizontal isothermal boundaries. Brass water jackets were clamped onto both the lower and upper copper shims. Water, held at two selected constant temperatures by thermostats within $\pm 0{\cdot}01$ K, was circulated through the lower and upper jackets respectively. Owing to the high heat capacity of copper and brass the temperature difference across the cell was even more accurately maintained. The temperature difference ΔT between top and bottom boundaries was measured at three different locations using chromel–alumel thermocouples embedded in the copper shims. The temperature along the length b was found constant to $\pm 0{\cdot}005$ K within the accuracy of measurement. Low conductivity polyvinyl chloride plastic endwalls were used to confine the fluid layer inside the large horizontal extent b of the test cell. The shims and brass jackets were imbedded in big blocks of polyvinyl chloride plastic. The frame of the box, made of low-conductivity material (Novotex), had on each side a second glass window to insulate the cell from convective disturbances in the ambient air. Additional big pieces of high-density extradense polystyrene foam of low thermal conductivity helped reduce the convective heat exchange with the surrounding air to a minimum. These foam pieces were temporarily removed when interferograms were taken. Water and silicone oils (M3 and M10) were used as test fluids, the pertinent properties of which are listed in table 1.

As pointed out by Elder (1967*a*), Davis (1967) and Stork & Müller (1972), the axes of the two-dimensional roll cells always align themselves parallel to the shorter horizontal dimension of the test cell. The test cell was placed in a holographic real-time interferometer (Koster 1980), with the optical path arranged parallel to the roll axes. With this arrangement and with infinite fringe adjustment (i.e. fringes very widely spaced) of the interferometer, the temperature fields, i.e. isotherms, of a section of the Hele-Shaw cell can be directly visualized and continuously recorded. A typical interferogram with a sketch of the streamlines of the convective flow in a Plexiglas-bounded Hele-Shaw cell is given in figure 2. Without incorporating correction terms, the equation correlating the number of fringes S in the interferogram and the temperature difference ΔT of (4) is

$$S = \frac{d}{\lambda}\frac{dn}{dT}\Delta T \tag{5}$$

(Hauf & Grigull 1970), where λ is the wavelength of the monochromatic light source and dn/dT the temperature dependence of the refractive index n.

Special care must be taken when optical measuring techniques are used to study convective flow in Plexiglas boxes (Koster 1980). Plexiglas has, in contrast to glass, a refractive index n that is strongly dependent on the temperature, i.e. $dn/dT = -1{\cdot}08 \times 10^{-4}\ \mathrm{K}^{-1}$ (while for glass $dn/dT = -5{\cdot}9 \times 10^{-6}\ \mathrm{K}^{-1}$; for water $dn/dT = -0{\cdot}98 \times 10^{-4}\ \mathrm{K}^{-1}$; and for silicone oil M3 and M10 $dn/dT = -4{\cdot}17 \times 10^{-4}\ \mathrm{K}^{-1}$). Therefore, the number S of fringes obtained in a convection box bounded by Plexiglas walls is proportional to the composite cell thickness Y, instead of the thickness d of the fluid layer only as shown in (5). The temperature dependence dn/dT of the refractive index must then be integrated across the thickness Y along the optical path. In this way the interferograms obtained actually contain information on the temperature fields of both the fluid layer and the walls. In the high-aspect-ratio Hele-Shaw cells discussed here, the convective flow imposed its temperature field on the Plexiglas walls, which was visualized in the form of additional fringes. These additional fringes allowed a very accurate measurement of the onset of convective flow, since the fluid integration length d was not long enough

Material	Copper	Glass BK7	Plexiglas	Water (T in °C)	Silicone oil M 3	Silicone oil M 10
ρ (kg/m^3)	8900	2510	1180	$1002{\cdot}75\exp(-2{\cdot}244\times10^{-4}T)$	$909{\cdot}80\exp(-1{\cdot}025\times10^{-3}T)$	$955{\cdot}03\exp(-1{\cdot}009\times10^{-3}T)$
c_p (Ws/kg K)	383·1	856·9	1470	4181·8	1507	1507
β (K^{-1})	—	—	—	$(0{\cdot}09T+0{\cdot}3)\times10^{-4}$	$(1{\cdot}105T+999{\cdot}9)\times10^{-6}$	$(1{\cdot}048T+999{\cdot}2)\times10^{-6}$
κ (m^2/s)	$1{\cdot}13\times10^{-4}$	$5{\cdot}17\times10^{-7}$	$1{\cdot}09\times10^{-7}$	$1{\cdot}31\times10^{-7}\exp(4{\cdot}25\times10^{-3}T)$	$7{\cdot}636\times10^{-8}\exp(1{\cdot}025\times10^{-3}T)$	$9{\cdot}695\times10^{-8}\exp(1{\cdot}008\times10^{-3}T)$
ν (m^2/s)	—	—	—	$1{\cdot}679\times10^{-6}\exp(-2{\cdot}559\times10^{-2}T)$	$4{\cdot}182\times10^{-6}\exp(-1{\cdot}617\times10^{-2}T)$	$14{\cdot}396\times10^{-6}\exp(-1{\cdot}750\times10^{-2})$
k (W/m K)	386	1·11	0·19	$0{\cdot}559\exp(3{\cdot}200\times10^{-3}T)$	0·105	0·140

TABLE 1. Properties and equations of state of materials used in the experiments: density ρ; specific heat c_p; coefficient of thermal expansion β; thermal diffusivity κ; kinematic viscosity ν; thermal conductivity k; temperature T in °C

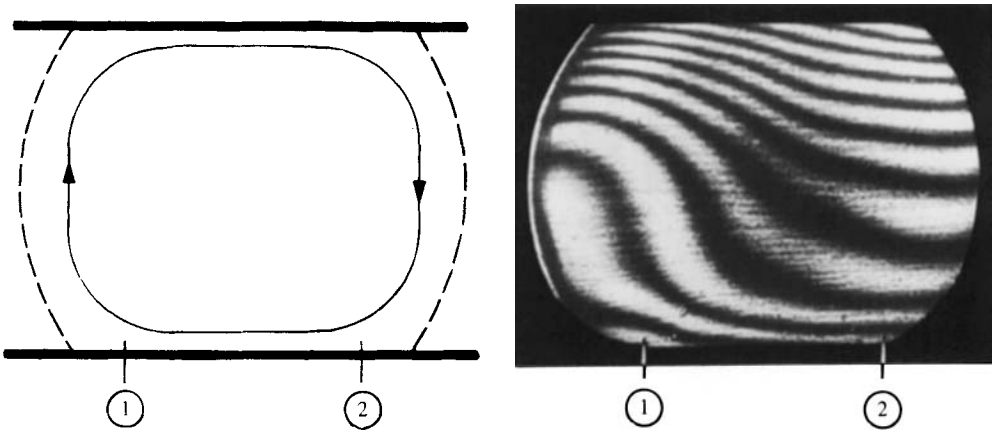

FIGURE 2. Typical interferogram and corresponding schematic streamline of convective flow indicating the observed wavenumber. Numbers indicate location of thermocouples in the gap: 1, location near upward flow; 2, location near downward flow. Dashed lines indicate visualization boundaries.

to generate even one single fringe at the critical temperature difference ΔT_c (cf. (5)). On the other hand, the presence of additional fringes from the sidewalls means that time-dependent flow phenomena cannot be effectively visualized at high Rayleigh numbers. Furthermore, Plexiglas absorbs fluid unevenly, causing non-uniform local changes of its optical properties. All optical properties of Plexiglas were taken into account during the experiments and in the interpretation of the results. It was also possible to evaluate the information on heat transfer in the cell from such interferograms (Koster 1982).

The fringe contribution of the sidewalls is negligible when glass is used. Then, interferograms show solely phenomena of the fluid layer. With the sensitivity of the present interferometer set-up the interferometric determination of the onset of convection in a glass box of small gap width d is limited to low aspect ratio h/d.

Because of the difficulties in determining an integral value of dn/dT to evaluate ΔT in (5), the temperature difference across the layer was measured by thermocouples. Since cellular convection is inhibited by lateral walls (Catton & Edwards 1967; Frick & Clever 1982), the critical temperature difference for the onset of convection is high for boxes of high aspect ratio and low gap width. This is especially true for Hele-Shaw cells with $d \approx 1$ mm. For example, the critical temperature difference was $\Delta T_c = 6{\cdot}1$ K in a Plexiglas box of aspect ratio $h/d = 20{\cdot}2$ ($d = 1{\cdot}05$ mm). With the high controllability of the thermostats ($\Delta T < \pm 0{\cdot}005$ K), the measuring accuracy for the critical temperature difference is assumed to be better than $\pm 0{\cdot}2$ K, which is indicated by the size of the symbols used in figure 3. This is the overall accuracy for large aspect ratio h/d in combination with a small gap width d (≈ 1 mm), or low aspect ratio with a large gap width d (≈ 3 mm), taking into account the interferometer sensitivity.

Another peculiarity of Plexiglas that has to be considered when investigating convection in Hele-Shaw cells is its low thermal diffusivity κ compared with that of the fluids used. For example, for a height $h = 30$ mm the thermal diffusion time in Plexiglas is $h^2/\kappa_s \approx 4$ h, and in water $h^2/\kappa_f \approx 3$ h. As a quasi-steady temperature increase had to be matched closely, the heating rate applied to the layer was carefully

chosen according to these diffusion times. Generally, the temperature difference was adjusted about every 6 h by 0·1 K at a feasible minimal heating rate of about 0·01 K/min. Consequently the experiments in which the marginal state was approached from below were extremely lengthy, requiring up to 40 days for the collection of the whole set of experimental data shown in figure 3.

In Hele-Shaw cells the very large contact area of the small fluid volume and the low conductivity sidewalls have even more implications on quasi-steady heating conditions. When a slight transient heating rate is applied to the bottom of the cell the temperature propagates significantly faster through the fluid than through the Plexiglas walls, causing heat transfer between the fluid and the Plexiglas. For an experimental simulation of the ideal condition of adiabatic sidewalls, the temperature profile of the convection layer would have to be realized in the Plexiglas in order to generate local thermal equilibrium at the wall–liquid interface. In the experimental determination of the marginal state of onset of convection, the relaxation times for achieving the required local thermal equilibrium are different depending on whether the marginal state is approached from subcritical or supercritical Rayleigh numbers. Owing to the faster convective heat transfer and the shorter transverse diffusion time $(Y-d)^2/4\kappa_s$ (which is, for example, 5·5 min for 6 mm thick Plexiglas) the thermal relaxation time is considerably smaller for the fluid. In experiments these circumstances can result in different measured values of the critical Rayleigh number, as will be discussed in §3.

In Hele-Shaw cells bounded by high-conductivity glass walls with $h^2/\kappa_f \gg h^2/\kappa_s$, the propagation of the temperature is much faster in the glass walls than in the fluid. Thus heat is normally transferred through the glass walls into the fluid, and the temperature profile in the walls is maintained practically linear at any given time during slight transient heating processes. Since the condition $(\frac{1}{2}d)^2/\kappa_f \ll h^2/\kappa_s$ holds, a quasi-steady heating rate can be achieved in these cells more easily than in Plexiglas cells.

Time-dependent convective-flow phenomena have been studied interferometrically in a Hele-Shaw cell of geometrical aspect ratios $h/b/d = 0{\cdot}16/1/0{\cdot}007$ ($h/d = 23$) and $Y/d = 4{\cdot}9$ ($d = 3{\cdot}05$ mm) bounded by Plexiglas walls. Because of the optical properties of Plexiglas discussed above, visual information about convective processes in time intervals smaller than $(Y-d)^2/4\kappa_s$ is suppressed. Therefore two thermocouples 0·25 mm thick were inserted into the fluid (see figure 2) in order to measure time-dependent phenomena in the fluid (water). One thermocouple projected about 2 mm into the fluid as the sensor and the other was embedded in the copper shims along the same vertical axis. The close mounting of the reference thermocouple was chosen to minimize the d.c. offset of the thermocouple signal. The time-dependent signals were recorded on tape for as long as 12 h at a fixed Rayleigh number. The frequency spectra of those signals were obtained by a digital fast Fourier analysis of 8192 samples or less; for details see Koster (1980). Frequencies with discrete power could be determined with an accuracy of $\pm 2 \times 10^{-5}$ Hz, depending on the Nyquist frequency. The centre-frequency of bandpass noise was determined indirectly with the half-width at about $\frac{1}{10}$ of maximum power. The accuracy of this determination depends on the shape of the noise spectrum, but is considered to be $\pm \Delta f = 10^{-3}$ Hz. The first-order error of the determination of the dimensionless period is $\Delta\tau = (\kappa/h^2)\,(1/f)\,(\Delta f/f)$, which assumes the values $\pm \Delta\tau = 8 \times 10^{-5}$ at the first observed bandpass noise and $\pm \Delta\tau = 3{\cdot}3 \times 10^{-5}$ at $Ra^* = 3{\cdot}2$ respectively. This error is smaller than the symbol size in the logarithmic plot of figure 7. Additional errors, which are not quantified, may be related to the development of the flow in the finite cavity.

A second, similarly arranged pair of thermocouples was mounted at a distance of

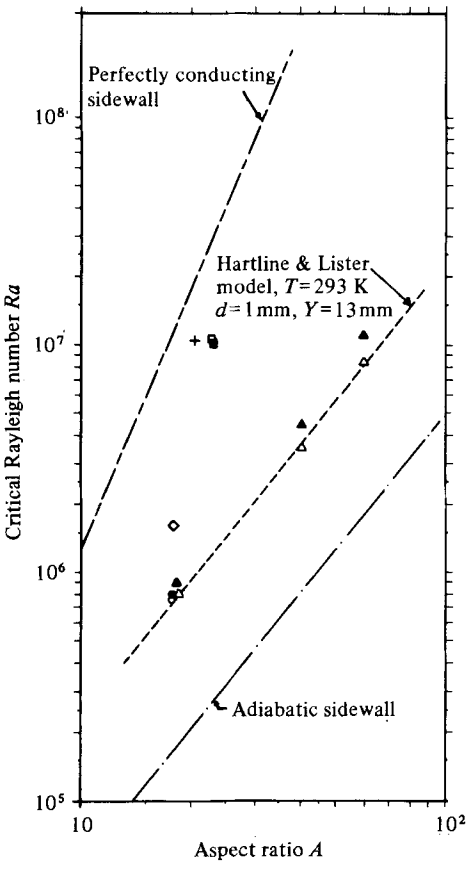

FIGURE 3. Critical Rayleigh number versus aspect ratio $A = h/d$ for different gap widths d, different materials of the sidewalls and different fluids. Experimental results are indicated by symbols explained in table 2. The theoretical results of Hartline & Lister (1977) and Frick & Clever (1980) are displayed by dash and dash-dotted lines.

60 mm to the side of the first set, so that the spacing between the two pairs of thermocouples was less than the height $h = 70$ mm of the test cell. This spacing is slightly smaller than half the wavelength of the convective rolls of critical wavenumber.

3. Onset of convection

The onset of convection in the fluid layer within the gap was determined by increasing and/or decreasing the temperatures at the lower and/or upper boundaries of the test cell in small steps and by simultaneously observing changes in the fringe pattern of the real-time interferograms. The marginal state was approached repeatedly by increasing the temperature difference ΔT between bottom and top of the layer starting from the state of pure heat conduction, and by decreasing ΔT starting from a state of slow convective motion. The onset of convection was defined when the parallel fringe pattern of the state of pure heat conduction was slightly deformed to a wavy shape indicating the appearance of vertical flow components and the development of a regular pattern of wavenumbers. The temperature differences applied to the cell at these states were plotted versus developing wavenumbers. The minimum of the envelope to the experimental data allows an accurate determination

Material of sidewalls	Fluid	$\frac{1}{2}(Y-d)$ (mm)	h (mm)	d (mm)	Ra (4)	Ra^{HL} (6)	Symbol in figure 3	Conditions
Plexiglas	Water	6	20·20	1·05	$11{\cdot}3\times10^6$	53·1	▲	*Ra* increasing
					$8{\cdot}5\times10^6$	39·9	△	*Ra* decreasing
Plexiglas	Water	6	41·02	1·02	$3{\cdot}8\times10^6$	41·0	▲	*Ra* increasing
					$3{\cdot}6\times10^6$	39·0	△	*Ra* decreasing
Plexiglas	Water	6	60·30	1·00	$8{\cdot}9\times10^5$	46·0	▲	*Ra* increasing
					$8{\cdot}0\times10^5$	40·6	△	*Ra* decreasing
Plexiglas	Water	12	20·83	1·15	$7{\cdot}76\times10^5$	26·7	●	*Ra* increasing
					$7{\cdot}50\times10^5$	25·8	○	*Ra* decreasing
Glass	Water	12	20·58	1·15	$1{\cdot}6\times10^6$	10·8	◇	
Glass	Silicone oil M3	12	20·70	1·00	$10{\cdot}5\times10^7$	7·4	+	*Ra* increasing or decreasing
Glass	Silicone oil M3	12	70·55	3·05	$10{\cdot}7\times10^7$	18·3	□	
Glass	Silicone oil M10	12	70·55	3·00	$10{\cdot}2\times10^7$	16·6	■	

TABLE 2. Dimensions and properties of the Hele-Shaw cells. The critical Rayleigh numbers are calculated from experimental data according to the definitions given by (4) and (6). $\frac{1}{2}(Y-d)$ is the thickness of the sidewalls; h is the layer height; d is the gap depth.

of the critical Rayleigh number and critical wavenumber in the Hele-Shaw cells. When the temperature difference ΔT was reduced, the termination of convective flow was defined when a pattern of horizontal parallel fringes reappeared in the interferogram.

The critical Rayleigh numbers evaluated in this way are displayed as a function of the aspect ratio $A = h/d$ in figure 3, in which the experimentally determined values are indicated by the different symbols. The experimental errors remain within the size of each of the symbols, which corresponds to an accuracy of $\pm 0{\cdot}2$ K of the temperature measurements (see §2). The theoretical predictions of Frick & Clever (1980) are indicated by the dashed and dash-dotted curves. These curves describe the onset of convection for either perfectly conducting or adiabatic sidewalls. The theory predicts that for $A > 10$ the critical Rayleigh number varies as $Ra \propto A^4$ or $Ra \propto A^2$ for perfectly conducting or adiabatic sidewalls respectively. In the experiments, these two ideal situations, namely the perfectly conducting and adiabatic sidewalls, can only be approximated by choosing appropriate combinations of the thermal properties of the fluid and the sidewall material.

The value of the ratio of the thermal conductivities of the wall material to the fluid gives an indication of the closeness of the actual vertical boundary condition to those of the ideal cases. The different combinations of wall material and fluid covered in the experiments are described in table 2. The combination of high-conductivity glass and low-conductivity silicone oil may be considered to provide a reasonable simulation of the ideal case of perfectly conducting boundaries. This is evidenced by the close agreement between the experimental values of the critical Rayleigh number for this case and the theoretical predictions for perfectly conducting sidewalls. The combination of water, which has a higher thermal conductivity than silicone oil, as the test fluid and glass plates as the sidewalls yields values of the critical Rayleigh number lower than those for the case of silicone oil and glass, but higher than those for the case of water and Plexiglas. The Plexiglas used as the wall material provides insulation while allowing flow visualization. The values of the critical Rayleigh number for this case are found to be closer to the adiabatic lower bound given by the theory of Frick & Clever (1980).

From theoretical considerations it is to be expected that the onset of convection does not exhibit hysteresis effects; i.e. the principle of exchange of stabilities should apply. In the experiments using glass sidewalls the critical Rayleigh numbers were found, within experimental error, to be independent of the way the onset of convection was determined; whether by quasi-steady increase or decrease of the temperature difference ΔT. In the experiments with Plexiglas walls, however, owing to the thermal interaction of the Plexiglas walls and the water discussed in §2, differences of about 30% were observed in the experimentally determined critical Rayleigh numbers, depending on whether the marginal state was approached from below or from above.

For comparison, the critical Rayleigh number according to the model of Hartline & Lister (1977) for one special value of $\epsilon = d/Y$ is also shown in figure 3. They used a Rayleigh number

$$Ra^{\mathrm{HL}} = \frac{\beta g \Delta T h}{\kappa_{\mathrm{m}} \nu} \frac{d^3}{12\,Y}. \tag{6}$$

According to this definition the following correlation between (4) and (6) should hold:

$$Ra_{\mathrm{c}} = 4\pi^2 \frac{Y}{d} \frac{\kappa_{\mathrm{m}}}{\kappa_{\mathrm{f}}} \left(\frac{h}{d}\right)^2, \tag{7}$$

where the factor $4\pi^2$ is the value for the critical Rayleigh number Ra_c^{HL} as calculated for a porous medium (Lapwood 1948). The slope of the curve corresponding to (7) indicates that only those cases in which adiabatic walls are approximated in the experiment can be reasonably described by this equation.

The values of critical Rayleigh number Ra_c^{HL}, (6), calculated with the measured critical temperature difference ΔT_c, are displayed in table 2. If the Rayleigh number of Hartline & Lister should be applicable in general, the critical value Ra_c^{HL} would have to be $4\pi^2$ for all cases investigated. However, this is only true for those arrangements of the Hele-Shaw cells that correspond to the experimental set-up employed by Hartline & Lister in their experiments. Discrepancies exist for the other cases of arrangements of Hele-Shaw cells. For example, when the thickness of the Plexiglas windows were increased to 12 mm, no substantial difference in the critical temperature difference was found, provided that the aspect ratio h/d and the gap width d were the same. According to (6), however, the critical temperature difference should be higher as $Ra_c^{HL} \propto \Delta T_c / Y$.

The results of our experimental investigation were as expected, since it was observed in other investigations that lowering the heat conductivity of the bounding walls reduces the critical Rayleigh number (see e.g. Sparrow, Goldstein & Jonsson 1964). Thus the experimental critical Rayleigh numbers obtained with materials of finite heat conductivity will have as upper or lower bounds the ideal cases of either perfectly conducting or adiabatic sidewalls considered in the theory of Frick & Clever (1980).

4. Stability of two-dimensional convection

The stability of a free convective flow is usually described by stability diagrams, in which stable and unstable states are separated by bounding curves of marginal stability relating the Rayleigh numbers to the wavenumbers. The validity of the Hele-Shaw approximation of convection in porous media at supercritical Rayleigh number has been discussed by Frick & Clever (1980).

Kvernvold (1979), Frick & Clever (1980) and Frick (1981) have calculated stability diagrams for finite-amplitude two-dimensional convection in Hele-Shaw cells. Their theoretical findings are presented in figure 4 together with our experimental results. In the graph of figure 4 the different states of the fluid flow are characterized by the ratio Ra/Ra_c of the actual Rayleigh number to the critical Rayleigh number, and the ratio α/α_c of the actual wavenumber to its critical value. From an experimental point of view, this way of plotting the results removes in part the influence of the thermal properties of the sidewalls and thus presents the data in a more general form. The dash-dotted curve of marginal stability separates the range of convection from states of pure heat conduction. According to the theory of Eckhaus (1965), two-dimensional finite-amplitude convection, whose wavenumbers fall in the sidebands of the amplified spectrum of the linearized stability theory, is unstable to other two-dimensional disturbances of wavenumbers close to the critical value. The limit line of the so-called Eckhaus instability is indicated in figure 4 by the solid lines. Oscillatory convective flow is to be expected for supercritical Rayleigh numbers beyond the dashed curve for oscillatory instability. According to these predictions, stable steady two-dimensional convection can only occur within the range of Rayleigh number and wavenumber ratios bounded by the solid and the dashed curves in the graph.

In order to check these predictions, several experiments were carried out employing

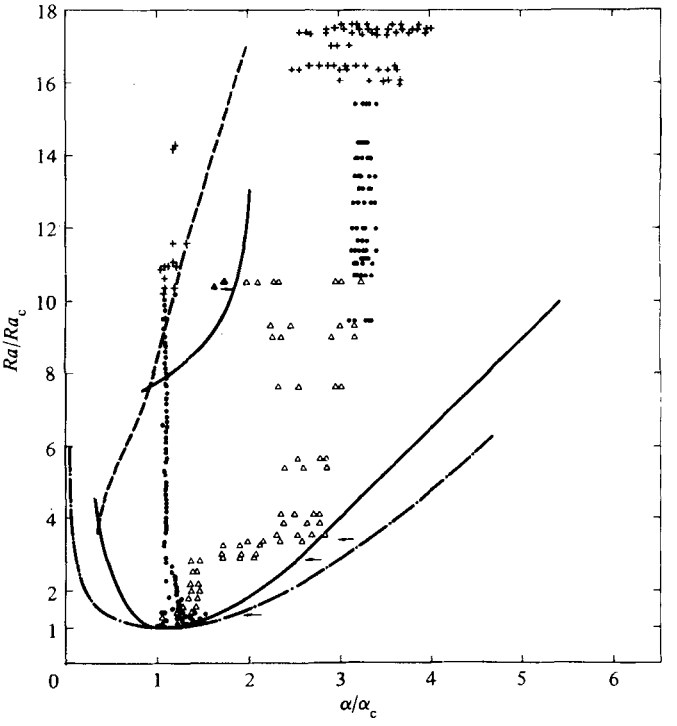

FIGURE 4. Stability diagram. Normalized Rayleigh numbers versus normalized wavenumbers. Experiments are performed in a Hele-Shaw cell with Plexiglas sidewalls and water as the test fluid. Dimensions of the cell: $h/d = 41{\cdot}0$, $Y/d = 13$, $h/b = 0{\cdot}095$. Range of the variation of the Prandtl number: $5{\cdot}00 < Pr < 7{\cdot}37$. Theoretical results of the works of Kvernvold (1979) and Frick (1981) on the Eckhaus and oscillatory instabilities are indicated by the solid (—) and dashed (– – –) curves respectively; –·–·–, neutral curve for onset of convection. Experimental results are indicated by symbols: ●, stable steady states established for increasing Ra/Ra_c; △, stable steady states for decreasing Ra/Ra_c; ▲, transient states; +, oscillatory states.

one special Hele-Shaw cell that had the geometrical dimensions $h/d = 41{\cdot}0$, $h/b = 0{\cdot}095$ and $Y/d = 13$. The sidewalls consisted of Plexiglas plates of 6 mm thickness and the gap of 1 mm width was filled with water. In a first extensive experiment,† starting from critical conditions – illustrated by the row of circular symbols in the left portion of figure 4 – the temperature difference between the lower and upper boundaries of the layer was increased in a quasi-steady way similar to the procedure described in §3. It was observed that, during the quasi-steady heating, adjacent convective roll cells usually had slightly different wavenumbers. Nevertheless, without changing the mean wavenumber, the flow maintained stable steady states up to $Ra/Ra_c \approx 10$. On exceeding this value, non-steady oscillatory phenomena were first observed close to the lower boundary of the apparatus. When the Rayleigh number was slightly increased, similar unsteady phenomena also occurred at the upper boundary. This small shift in the Rayleigh numbers can be attributed to slightly different local thermophysical properties of the fluid near the lower and upper boundaries owing to the temperature variation across the layer. The oscillatory phenomena increased in intensity and frequency of occurrence when the Rayleigh

† The time period for the different experiments reported here were between 20 and 25 days each.

number was increased further. In the graph of figure 4, the conditions where oscillatory flow was observed are marked by crosses. The flow oscillations vanished without a pronounced hysteresis effect when the Rayleigh numbers were reduced below the value $Ra/Ra_c = 10$. However, before a hysteresis effect for the transition from steady-state flow to oscillatory flow and then back to steady-state flow can be excluded, more careful experiments will have to be performed. More details about the character of the oscillatory flow are presented in §5.

A comparison between the experimental findings and the theoretical predictions shows that oscillatory states are found to occur just above the bounding curve for oscillatory instability. This can be regarded as qualitative agreement between experiment and theory. On the other hand, it is surprising to note that steady-state convection was observed in the range of Rayleigh numbers between the curve of Eckhaus and the curve of oscillatory instability. According to the stability calculations of Kvernvold (1979) and Frick (1981) one would have expected that in this unstable range transient states of convection should occur, shifting the wavenumbers of the cell to higher stable values. This discrepancy may be explained by the following reasoning. As briefly outlined in §3, it has been repeatedly observed that the temperature field of the fluid flow is stored in the Plexiglas walls (Koster 1980). This stored temperature profile reduces disturbances in the flow that could otherwise have changed the wavenumber during the observation and measuring time.

In a second experiment, the stability of steady-state convection flows of large wavenumbers (i.e. small cell sizes) was investigated at very high supercritical Rayleigh numbers. The results are represented by circular symbols in the middle and upper portion of figure 4. Starting from an isothermal fluid layer, a sudden temperature increase corresponding to a Rayleigh number $Ra/Ra_c \approx 9{\cdot}4$ was applied at the lower boundary of the fluid layer. By the transient heating a whole set of convection cells of different sizes were generated initially in the fluid layer. The cells gradually adjusted themselves to a mean size. After about one diffusion time $t_d = h^2/\kappa_f$, the wavenumbers of these cells were found to be in the range $3{\cdot}1 < \alpha/\alpha_c < 3{\cdot}4$. The wavenumbers of steady flow after a stepwise temperature increase are larger than the critical wavenumber α_c and conform to the findings of Elder (1968). Corresponding phenomena were observed by Koschmieder (1969) in fluid layers of large horizontal extent.

When the Rayleigh number was then gradually increased to higher Rayleigh numbers, the steady-state convective flow in the range $9{\cdot}4 < Ra/Ra_c < 16$ maintained essentially the initial pattern, i.e. the initial wavenumber. At Rayleigh numbers $Ra/Ra_c > 16$, time-dependent wave-like perturbations were first observed to occur near the lower heated boundary, and, at a slightly increased Rayleigh number, the analogous phenomena were found near the upper cooled boundary. Crosses in the upper portion of figure 4 mark the fluctuating cellular flow and indicate an increase in wavenumber bandwidth with increasing Rayleigh number. The time-dependent events represent a change of the wavenumbers of some convection cells to smaller or larger values at the expense of their neighbouring cells caused by the strongly unstable boundary layers. But the basic convection mode, which circulates fluid from the bottom to the top of the cell and vice versa, continues to dominate the flow. Similar phenomena have also been observed by Krishnamurti (1973) in fluid layers of large horizontal extent.

Although the transition from steady convection flows to unsteady flow at very high Rayleigh numbers and very small cell sizes is to be expected, the threshold Rayleigh number obtained from the experiments is considerably smaller than an extrapolation

of the curve of oscillatory instability in the graph would predict. Further investigations are needed to clarify whether the extrapolation of the theoretical results is valid, and whether the relatively early onset of oscillatory flow in the experiment may have been caused by experimental deficiencies, e.g. end effects (finite length of the cell) within the Hele-Shaw cell.

A third experiment of long duration was again started by a sudden stepwise increase of the temperature at the lower boundary of the layer. Then, beginning at $Ra/Ra_c = 10{\cdot}3$, the Rayleigh number was decreased quasi-steadily. The observed wavenumbers are represented by triangular symbols in the middle and lower portion of figure 4. As in the second experiment, a set of convection cells of different sizes developed first. At the cessation of the fast transient process the wavenumbers of two of the simultaneously visualized convection cells were first found to be outside the bounding curve of the Eckhaus instability. In the following slow transient process lasting for about one diffusion time $t_d = h^2/\kappa_f$, the wavenumbers of these two cells shifted to higher values and into the range of stable steady convection. This event is indicated in figure 4 by the two solid triangles and the arrow. The experiment was then continued by quasi-steadily reducing the temperature difference between bottom and top of the fluid layer. Steady-state convection was found for all Rayleigh numbers down to a value $Ra/Ra_c = 3{\cdot}5$. At this value one of the largest wavenumbers observed in the Hele-Shaw cell touched the bounding line of the Eckhaus instability. When the Rayleigh number was decreased further, the fluid system in the Hele-Shaw cell reacted by reducing the wavenumbers of all convection cells. This occurred in a transient process during which several (one or more) convection cells in the fluid system were destroyed. This phenomenon was repeated in two more steps, when the Rayleigh number was reduced even further, until finally the critical conditions $Ra/Ra_c = 1$ and $\alpha/\alpha_c = 1$ were reached. The stepwise reductions in the wavenumbers are indicated in figure 4 by arrows on the right branch of the curve of Eckhaus instability. More details of the change of wavenumbers can be seen from the interferograms in figure 5. It can be recognized that the cell sizes increase distinctly during each of the three steps.

The stepwise reduction of the wavenumbers in the range of Rayleigh numbers $3{\cdot}5 < Ra/Ra_c < 1$ is considered to be essentially a confirmation of the validity of the curve of Eckhaus instability in this range. One may argue that the experimental points meet the theoretical curve closely only for $Ra/Ra_c = 3{\cdot}5$, and are otherwise found remote from it. However, this effect can be attributed to the finite horizontal length of the Hele-Shaw cell, in which only a finite number of convection cells can be established for a particular Rayleigh number. End effects of the vertical sidewalls were found to quantize the wavenumbers within the system for certain intervals of Rayleigh numbers. Quantization has been observed by Bergé (1979) and Maurer & Libchaber (1979) in their experiments on Bénard convection. In addition, rolls of various wavenumbers coexisting at a particular Rayleigh number in the Hele-Shaw cell cause inhomogeneities of the flow pattern and the temperature fields (heat transfer). These perturbations may initiate the change of wavenumbers at Rayleigh numbers different from the marginal values of the Eckhaus-instability line. It is therefore reasonable to assume that, if the Hele-Shaw cell had been of infinite extent and if the rolls had equal size, then the change of the wavenumbers would have occurred along the theoretical curve of the Eckhaus instability.

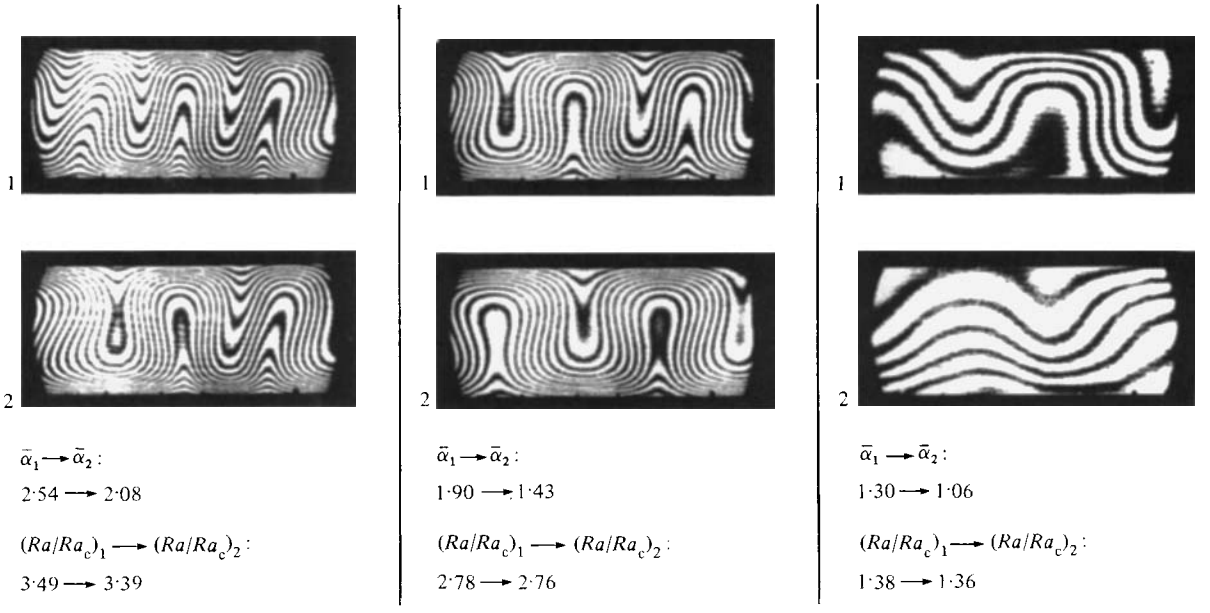

FIGURE 5. Interferograms illustrating the change of the mean wavenumber $\bar{\alpha}$ in the Hele-Shaw cell occurring close to the curve of Eckhaus instability for decreasing Rayleigh numbers given in figure 4.

5. Time-dependent flow

In this section the oscillatory convective flow at high Rayleigh numbers will be discussed in more detail. The Hele-Shaw cell with low-conductivity Plexiglas sidewalls used for these investigations is described in §2.

The oscillations of the flow were found to set in at a well-defined Rayleigh number $Ra_{\mathrm{osc}} = 5{\cdot}96 \times 10^6$. Increasing and decreasing the temperature difference across this threshold did not reveal a hysteresis. Wavy perturbations were observed to occur repeatedly close to the heated lower and cooled upper boundaries of the layer, which is a characteristic feature of the oscillatory convective flow in a Hele-Shaw cell. The chronological development of a typical perturbation is shown in figure 6 by a sequence of interferograms of one cell section close to the lower boundary. These perturbations, which can also be interpreted as small vortices, are always generated near the stagnation point of the downflowing (upflowing) convective jet (figure 6*a*), where the thickness of the thermal boundary layer was smallest. An estimate of the local boundary-layer thickness δ can be obtained from the visualized height of the vortices. After generation, these vortices convect sidewards and away from the horizontal boundary by the main flow of the convection cell. Moving along the horizontal boundaries, the vortices grow in size. When the Rayleigh number is increased, the region of occurrence of such vortices becomes smaller as the boundary-layer thickness δ is reduced, until finally it is of the same order as the gap width: $\delta \approx d$. Simultaneously the frequency of vortex generation increases, and several vortices may coexist momentarily in the horizontal boundary layers of a single convection cell.

It was estimated from the observation of the real-time interferograms that the extent of the perturbations was always limited to areas of densely packed fringes, i.e. to the thermal boundary layer. This suggests that the onset of oscillatory flow

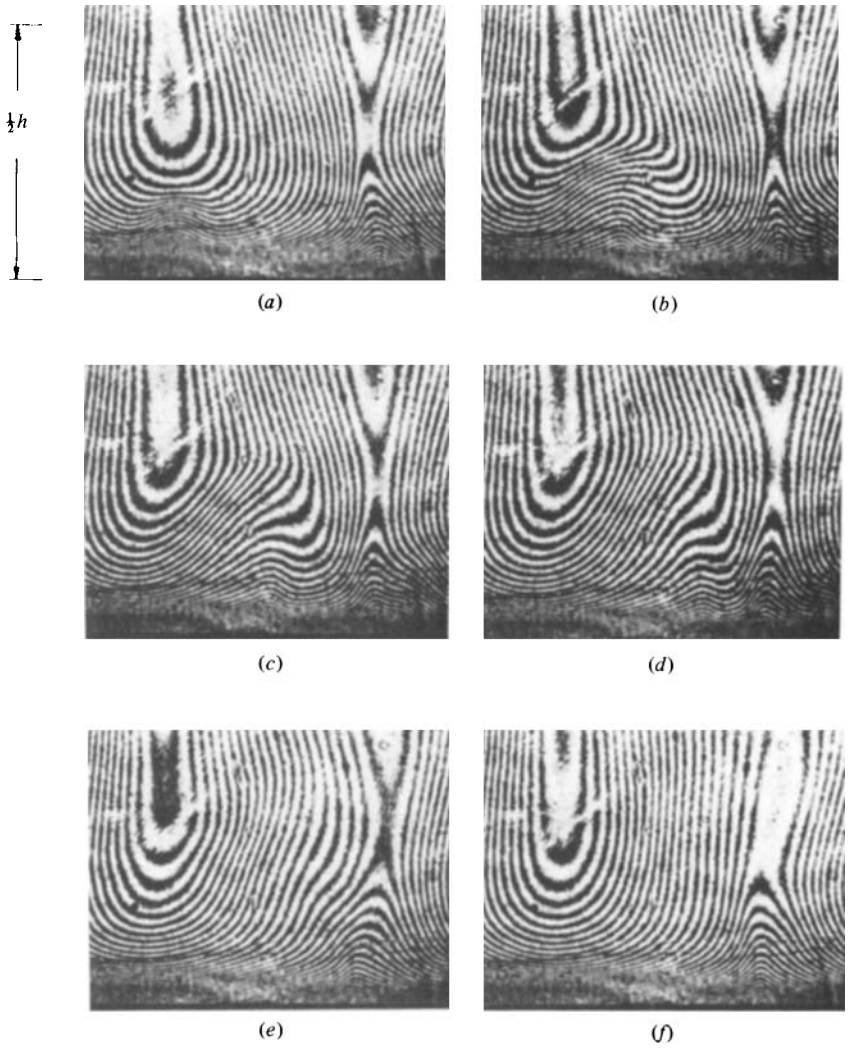

FIGURE 6. Interferograms illustrating the time-dependent perturbation of the thermal boundary layer near the lower horizontal wall. Experimental data: $Ra/Ra_c = 11{\cdot}8$; $h/d = 66{\cdot}5$; $Y/d = 25$; lifetime of an individual perturbation, 240 s.

could be explained by an instability of the thermal boundary layer. For infinitely extended horizontal fluid layers heated from below, this idea was first expressed by Howard (1964) and repeatedly experimentally confirmed, e.g., by Busse & Whitehead (1974). An interferometric confirmation was first given by Chu & Goldstein (1973).

To the best of our knowledge, the idea that boundary-layer instabilities may be responsible for the fluctuations in the free-convection gap flow was first expressed by Caltagirone, Cloupeau & Combarnous (1971). Horne & O'Sullivan (1978) discussed the same concept of boundary-layer instability for porous-media flow, and studied the phenomenon numerically.

The idea of an instability of the temperature boundary layer causing the unsteadiness of the Hele-Shaw flow can be substantiated by similarity arguments analogous to those first applied by Howard (1964). Proceeding on the assumptions

that, at the high Rayleigh numbers under consideration, thermal boundary layers of thickness δ have developed along the horizontal walls, and that the thickness δ is still much larger than the gap width d, one may postulate that the analogy of Hele-Shaw flow to the flow in porous media even holds for the region of the boundary layer (Elder 1967*a*, *b*). Based on these ideas, a properly defined Rayleigh number for the region of this boundary layer would be, according to (3), $Ra^{\mathrm{HS}}(\delta) = \beta g K(\kappa_{\mathrm{m}}\nu)^{-1}\delta_2^1\Delta T$. Accepting the model that this boundary layer becomes unstable for values of $Ra^{\mathrm{HS}}(\delta)$ larger than a critical value, say $(Ra^{\mathrm{HS}}(\delta))_{\mathrm{c}} = 27$, the corresponding critical value for convection in a saturated porous medium (Lapwood 1948), we conclude, from the definition of $Ra^{\mathrm{HS}}(\delta)$, that the thickness of a stable boundary layer satisfies $\delta \propto \Delta T^{-1}$. As the growth of the thermal boundary layer at the horizontal walls results from heat conduction only, similarity considerations based on the heat-conduction equation lead to the following relation between the diffusion time for the temperature and the boundary-layer thickness: $t_{\mathrm{d}} \propto \delta^2$. A combination of these two relations and a substitution of ΔT by the Rayleigh number defined in (4) readily gives

$$\tau \propto Ra^{-2}, \tag{8}$$

where τ is defined as the dimensionless period of oscillation $\tau = (\kappa_{\mathrm{f}}/h^2)t$.

In order to quantify the interferometric observations of the flow fluctuations and to verify the idea of the unstable boundary layer, the temperature signals measured by sensors 1 and 2 (figure 2) were analysed. Hence 8192 digitized samples, from recordings of 5·8 h, were used to calculate the frequency spectra by fast Fourier transforms. The spectra showed discrete frequencies close to the threshold of oscillatory flow and bandpass noise at higher Rayleigh numbers. The evaluated frequency f was made dimensionless with the diffusion time h^2/κ_{f} of the fluid. The results were plotted in the form of the dimensionless period versus the normalized Rayleigh number Ra^*, which is defined as the ratio of the actual Rayleigh number to the Rayleigh number Ra_{osc} at the onset of the oscillations: $Ra^* = Ra/Ra_{\mathrm{osc}}$.

Figure 7 displays the experimental results and the piecewise least-square-fit curves for the measured centre-frequencies of the various regions for the purpose of comparing the results with the existing theories. For the various regions the following correlation formulas were found:

$$\tau = 4{\cdot}8 \times 10^{-3}(Ra^*)^{-1{\cdot}4} \quad (1 < Ra^* < 3{\cdot}2), \tag{9a}$$

$$\tau = 5{\cdot}4 \times 10^{-3}(Ra^*)^{-2{\cdot}0} \quad (1 < Ra^* < 1{\cdot}5) \quad \text{(I)}, \tag{9b}$$

$$\tau = 3{\cdot}4 \times 10^{-3}(Ra^*)^{-1{\cdot}0} \quad (2{\cdot}3 < Ra^* < 3{\cdot}2) \quad \text{(II)}. \tag{9c}$$

It is seen from figure 7 that at the beginning of the oscillations the period satisfies (8). The correlation coefficient was found closest to 1 when all the measuring points in the range $1 < Ra^* < 1{\cdot}5$ were taken into account. Also, in this range the smallest visualized thickness of the temperature boundary layer δ is still larger than the gap width d. The range II is defined somewhat arbitrarily by the experimental observation that the secondary vortices become so small that they can no longer be visualized by the interferometer. The time-dependent flow is then detected solely from thermocouple readouts. The interferogram shows a steady temperature field of the basic convective mode.

Stability arguments can also be used to explain the change of power of the experimental $\tau(Ra^*)$ correlation for high Rayleigh numbers. In this case the thickness δ of the boundary layer is comparable to or even smaller than the gap width d. Then

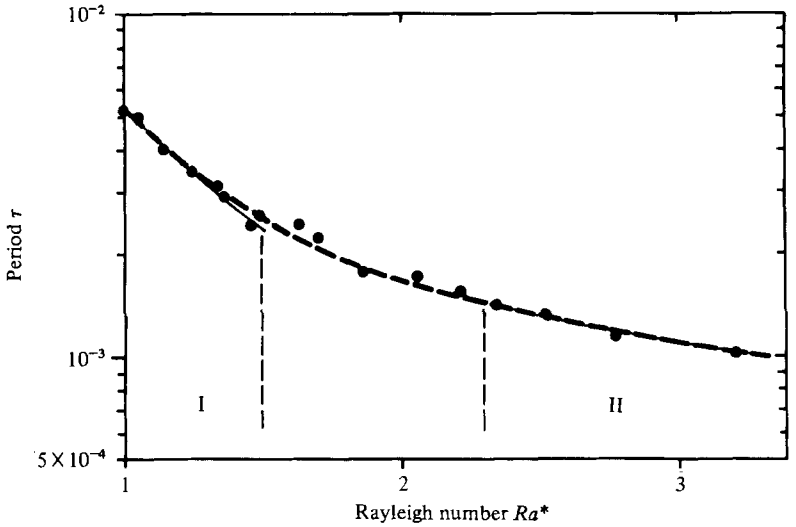

FIGURE 7. Non-dimensional periods of oscillation τ versus normalized Rayleigh number $Ra^* = Ra/Ra_{osc}$. Experiments are performed in a Hele-Shaw cell with Plexiglas sidewalls and water as the test fluid. Dimensions of the cell: $h/d = 23{\cdot}0$; $Y/d = 4{\cdot}9$; $h/b = 0{\cdot}16$. Curves give least-square fits of the experimental data: ---, fitted curve to all experimental data; —, fitted curve to the experimental data in sub-domains of Rayleigh numbers indicated by I and II.

the Hele-Shaw analogy to porous media no longer applies. For an assessment of the stability of the boundary layer it is reasonable to use now the classical definition of the Rayleigh number, given by (4) for the boundary-layer thickness δ, i.e. $Ra \propto \delta^3$. The same considerations as mentioned above then lead to the relation

$$\tau \propto Ra^{-\frac{2}{3}}, \tag{10}$$

which was first derived in this form by Howard (1964). This relation holds for infinitely extended layers according to Busse & Whitehead (1974) and for a confined box according to Dubois & Bergé (1981). Although experimental results are only available for $Ra^* < 3{\cdot}2$ it seems that the asymptotic behaviour of the periods of oscillations is qualitatively described by these considerations.

In their numerical investigations on convective flow in saturated porous media, Horne & O'Sullivan (1978) derived the law $\tau \propto Ra^{-1{\cdot}5}$ in a range of Rayleigh numbers Ra^* similar to that of our investigation. They associated the departure from the asymptotic relation $\tau \propto Ra^{-2}$ with an additional triggering mechanism by disturbances previously discharged from the thermal boundary layer and recirculated to their origin by the mean flow of the cell. In the present investigation, no evidence for triggering of instabilities was found, and thus this argument is not used to explain the power change of the $\tau(Ra)$ correlation.

Next, the frequency spectra of the flow oscillations will be discussed and related to visual observations of the interferograms. Some typical temperature signals from chart recorders and the corresponding power spectra (8192 samples) are displayed in figure 8. The temperatures were measured by thermocouples, whose positions in the flow are described in §2 and figure 2. Several intervals of the signals, recorded at constant Rayleigh number, were evaluated with 2048, 4096 and 8192 samples. A large number of spectra were taken for different Rayleigh numbers. From the analysis of the temperature histories and the power spectra, the following characteristic features were obtained:

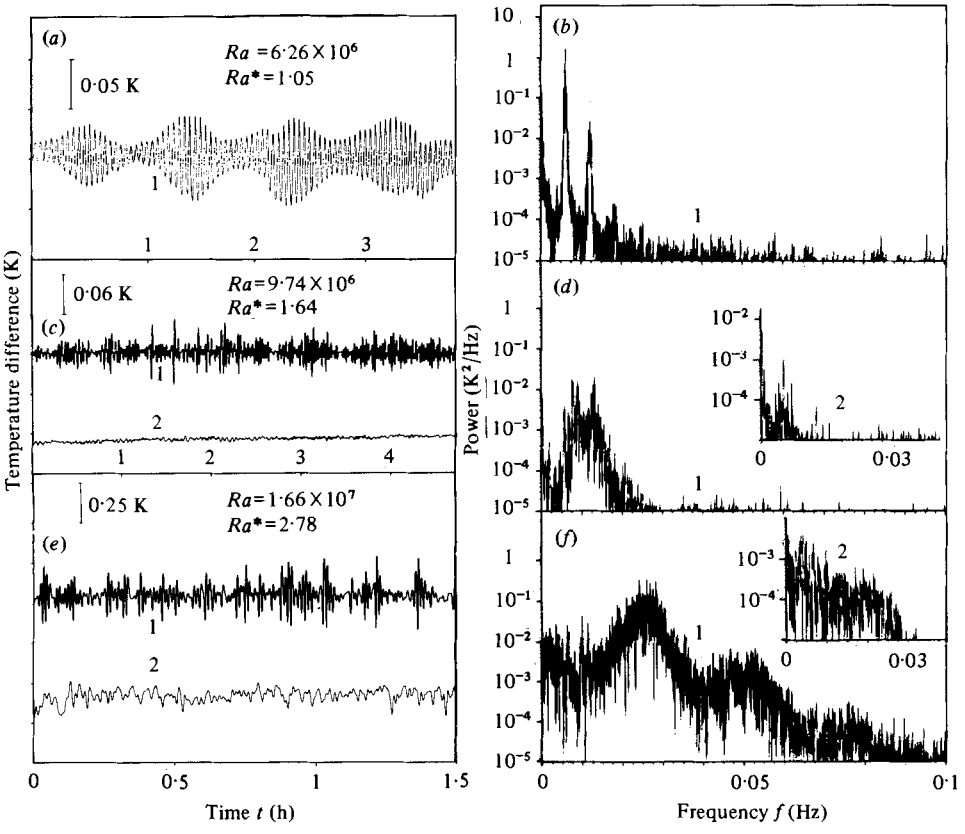

FIGURE 8. Temperature histories and corresponding power density spectra. Numbers 1 and 2 indicate signals from sensor locations 1 and 2 respectively, as explained in figure 2.

(i) In general, for long-time analysis, the time-dependent flow at any particular Rayleigh number shows stochastic features. A similar result for the time-dependent convective flow in a box of large horizontal extent has been reported by Ahlers & Behringer (1978*a*, *b*) and discussed by Busse (1981*a*, *b*).

(ii) Immediately beyond the threshold Rayleigh number of oscillatory flow, periodic or quasi-periodic motions develop (figure 8*a*). Some short time intervals (1 h) reveal periodic flow, whereas a long-time analysis (5·8 h) reveals a quasi-periodic oscillation. A high signal-to-noise ratio at the onset of oscillatory flow in the Hele-Shaw cell (figure 8*b*) decreases rapidly with increasing Rayleigh number. (The instrument noise was about 10^{-4} K²/Hz near zero frequency and decreased to about 10^{-5} K²/Hz at 0·1 Hz.) The energy becomes more uniformly distributed in the power spectrum. This is indicated by a rising bandpass noise.

(iii) In the range $1{\cdot}3 < Ra^* < 1{\cdot}64$ the noise develops strongly in the spectra. However, when comparing short-time (1 h) and long-time (5·8 h) analysis, one and, in some cases, two frequencies of highest amplitude can be evaluated from both sensor locations and for both long- and short- time analysis (figure 8*c*, *d*). The power spectra at both sensor locations exhibit basically the same shape of bandpass noise. The analog temperature signals show that the amplitude of the oscillations is smaller at sensor location 2, near the downward flow, than at sensor location 1, near the upward

flow. This supports the interferometric observation (figure 6) of the growth of the secondary vortices while moving from sensor location 2 to sensor location 1.

(iv) At even higher Rayleigh numbers, the oscillations have predominantly stochastic character (figure 8*e*). Even short-time analysis gives broadband spectra with no discernible single frequency. The spectrum of the temperature history from sensor 1 shows a bandpass noise with relative maxima, for which the centre-frequency can be evaluated (see §2 and figure 8*f*). It is remarkable that the bandpass noise in the spectra corresponding to sensor 1 exhibits harmonic bandpass noise. In contrast, the spectrum from the sensor location 2 reveals lowpass noise without maxima. Also, there is experimental evidence that this frequency band is bounded by a cutoff frequency, which increases with increasing Rayleigh number. Questions arise concerning the cause of the increasing amount of stochastic parts in the spectra and whether the sensor signals can be related to the visualized phenomena.

There is no doubt that the sharply defined frequency at the onset of oscillation obtained from the power-density spectrum of sensor 1 is directly related to the repeated occurrence of the wavy perturbations in the thermal boundary layer of the visualized roll cell. According to the previous discussions, these perturbations are generated near the stagnation points of the convection cells, where sensor 2 is located. The vortices then move towards the upflow after passing sensor 1. By counting these visualized events during a certain time interval or measuring the time interval between two events with a stop watch, the calculated frequency (figure 8*b*) could be confirmed. The vortices developing at one stagnation point may also at times move in a direction opposite to the usual one, i.e. penetrate into the boundary layer of the neighbouring roll cell, thereby introducing noise into the spectra. At very high Rayleigh numbers the horizontal boundary layers of each roll cell fill up with several vortices, which in another way contribute stochastic elements to the spectra.

Careful observation of the real-time interferograms revealed also that the cell sizes of the adjacent convection rolls were not absolutely constant at a particular Rayleigh number. Rather, the positions of the free boundaries of the convection cells fluctuate around a certain mean value. The fluctuations are most pronounced in regions close to the horizontal boundaries. In other words, convection cells expand temporarily at the expense of a neighbouring cell or give space to it. This effect can also be recognized from the interferograms in figure 6. These fluctuations appeared to have a regular character at the onset of oscillations and become more random at higher Rayleigh numbers. Visualizing the streamline pattern in a Hele-Shaw cell, Krishnamurti (1973) has observed similar phenomena.

Since a rigorous nonlinear theory for the phenomenon of cell size fluctuations is, to our knowledge, not available, some plausible arguments for its occurrence will be given below.

The experiments were performed in a Hele-Shaw cell of aspect ratio $b/h = 6$. This means that on the average there were six convection cells present in this Hele-Shaw cell. It is known from experiments in large containers (aspect ratio $b/h > 10$) that in general the wavenumber decreases (cell size increases) with increasing Rayleigh number (see e.g. Koschmieder 1966, 1969; Willis, Deardorff & Somerville 1972). When the temperature difference across the layer is increased, however, the number of convection cells is fixed for certain temperature intervals owing to the finite extent of the Hele-Shaw cell. An external constraint is thereby imposed on the system of convection cells. The fluid flow in the cells can be considered as 'thermally prestressed' and capable of responding readily to perturbations of the main flow. Initiated by the momentum transfer from the secondary vortices to the basic

convection roll, the main flow responds to this constraint by fluctuations of the cell sizes. It is conjectured therefore that these fluctuations are induced by the recurrent perturbations in the thermal boundary layers of the different convection cells.

In spite of the fact that the structure of the convective flow is essentially two-dimensional and characterized by slow motion, the flow nevertheless exhibits typical features of turbulence. First of all, the measurements indicate that the temporal structures of the signals from the probes show stochastic elements. Furthermore, the different cell sizes at any instant of time and the multiple secondary instabilities in the boundary layers necessitate the presence of a spectrum of intrinsic lengthscales within the two-dimensional flow.

6. Summary

Our experiments deal with steady and unsteady two-dimensional free-convective flows in Hele-Shaw cells of different dimensions. Transparent materials of different thermal properties were employed for the confining sidewalls of the cell and the fluid. Real-time holographic interferometry and spectrum analysis of temperature signals from thermocouples were the primary measuring tools.

Critical Rayleigh numbers for the onset of convection have been experimentally determined for different combinations of fluid and wall materials of the test cell. The experimental findings are consistent with theoretical results of Frick & Clever (1980) for the cases of perfectly conducting and adiabatic lateral boundaries of the Hele-Shaw cell. Special definitions of the Rayleigh number previously used by other authors to confirm the thermohydraulic analogy between Hele-Shaw convection and convection in porous media are shown to have no general application.

Using the Rayleigh-number ratios Ra/Ra_c and wavenumber ratios α/α_c, bounds of stability for two-dimensional steady convection were experimentally determined. The results are in fair agreement with the theoretical predictions of Kvernvold (1979), Frick & Clever (1980) and Frick (1981). The predicted oscillatory flow for high supercritical Rayleigh numbers was observed. Furthermore, the range of wavenumbers predicted by Eckhaus was confirmed in a certain range of wavenumbers and for moderately supercritical Rayleigh numbers.

It has been shown by flow visualization and supplemented by similarity considerations that two-dimensional oscillatory convection in a Hele-Shaw cell is initiated by an instability of the thermal boundary layers at the horizontal walls. The periods of oscillations decrease with increasing Rayleigh numbers. Close to the onset of oscillations the periods obey a power law valid for unsteady convective flow in a saturated porous medium. For very high Rayleigh numbers the correlation approaches the power law valid for the limiting case of the infinite layer.

The time-dependent phenomena have a periodic, quasi-periodic or stochastic behaviour. The predominant stochastic features are related to interactions between neighbouring convective cells and to the frequency of vortex generation in the boundary layer. Although the spectra of local temperature signals exhibit stochastic features, the character of the basic convection mode, i.e. the two-dimensional convection roll, is maintained.

The authors thank F. H. Busse, E. L. Koschmieder and R. S. Lee for valuable comments, which have greatly contributed to improving a previous draft of this article.

The financial support under Grant Mu 503 of the Deutsche Forschungsgemein-

schaft for major parts of this investigation is gratefully acknowledged. Support by the Crystal Growth Laboratory of the Department of Physics of the University of Utah for the first author (J.N.K.) during the writing of this paper is also gratefully acknowledged.

REFERENCES

AHLERS, G. & BEHRINGER, R. P. 1978*a* Evolution of turbulence from the Rayleigh–Bénard instability. *Phys. Rev. Lett.* **40**, 712–716.

AHLERS, G. & BEHRINGER, R. P. 1978*b* The Rayleigh–Bénard instability and the evolution of turbulence. *Prog. Theor. Phys. Suppl.* **64**, 186–201.

BEAR, J. 1972 *Dynamics of Fluids in Porous Media.* Elsevier.

BÉNARD, H. 1900 Les tourbillons cellulaires dans une nappe liquide. *Rev. Gen. Sci. Pur. Appl.* **11**, 1261–1271, 1309–1328.

BERGÉ, P. 1979 Experiments on hydrodynamic instabilities and the transition to turbulence. In *Dynamical Critical Phenomena and Related Topics* (ed. C. P. Enz). Lecture Notes in Physics, vol. 104, pp. 289–308. Springer.

BUSSE, F. H. 1981*a* Transition to turbulence in Rayleigh–Bénard convection. In *Hydrodynamic Instabilities and the Transition to Turbulence* (ed. H. L. Swinney & J. P. Gollub), pp. 97–137. Springer.

BUSSE, F. H. 1981*b* Transition to turbulence in thermal convection with and without rotation. In *Transition and Turbulence* (ed. R. E. Meyer), pp. 43–61. Academic.

BUSSE, F. H. & WHITEHEAD, J. A. 1974 Oscillatory and collective instabilities in large Prandtl number convection. *J. Fluid Mech.* **66**, 67–79.

CALTAGIRONE, J. P., CLOUPEAU, M. & COMBARNOUS, M. 1971 Convection naturelle fluctuante dans une couche poreuse horizontale. *C.R. Acad. Sci. Paris* B **273**, 833–835.

CATTON, I. & EDWARDS, D. K. 1967 Effect of side walls on natural convection between horizontal plates heated from below. *Trans. A.S.M.E.* C: *J. Heat Transfer* **89**, 295–299.

CHU, T. Y. & GOLDSTEIN, R. J. 1973 Turbulent convection in a horizontal layer of water. *J. Fluid Mech.* **60**, 141–159.

DARCY, H. 1856 *Les Fontaines Publiques de la Ville de Dijon.* Paris: Dalmont.

DAVIS, S. H. 1967 Convection in a box: linear theory. *J. Fluid Mech.* **30**, 465–478.

DUBOIS, M. & BERGÉ, P. 1981 Instabilités de couche limite dans un fluide en convection. Evolution vers la turbulence. *J. Phys. (Paris)* **42**, 167–174.

ECKHAUS, W. 1965 *Studies in Nonlinear Stability Theory.* Springer.

ELDER, J. W. 1967*a* Steady free convection in a porous medium heated from below. *J. Fluid Mech.* **27**, 29–48.

ELDER, J. W. 1967*b* Transient convection in a porous medium. *J. Fluid Mech.* **27**, 609–623.

ELDER, J. W. 1968 The unstable thermal interface. *J. Fluid Mech.* **32**, 69–96.

FRICK, H. 1981 Zellularkonvektion in Fluidschichten mit zwei festen seitlichen Berandungen. Dissertation, Universität Karlsruhe. *KfK-Rep.* nr. 3109.

FRICK, H. & CLEVER, R. M. 1980 Einfluß der Seitenwände auf das Einsetzen der Konvektion in einer horizontalen Flüssigkeitsschicht. *Z. angew, Math. Phys.* **31**, 502–513.

FRICK, H. & CLEVER, R. M. 1982 The influence of side walls on finite amplitude convection in a layer heated from below. *J. Fluid Mech.* **114**, 467–480.

GOLLUB, J. P. & BENSON, S. V. 1978 Chaotic response to periodic perturbation of a convecting fluid. *Phys. Rev. Lett.* **41**, 948–951.

GOLLUB, J. P. & BENSON, S. V. 1980 Many routes to turbulent convection. *J. Fluid Mech.* **100**, 449–470.

HARTLINE, B. K. & LISTER, C. R. B. 1977 Thermal convection in a Hele-Shaw cell. *J. Fluid Mech.* **79**, 379–389.

HARTLINE, B. K. & LISTER, C. R. B. 1978 An experiment to verify the permeability of Hele-Shaw cells. *Geophys. Res. Lett.* **5**, 225–227.

HAUF, W. & GRIGULL, U. 1970 Optical methods in heat transfer. *Adv. Heat Transfer* **6**, 133–366.

HELE-SHAW, H. S. 1898 The flow of water. *Nature* **58**, 34–36.

HORNE, R. N. & O'SULLIVAN, M. J. 1974 Oscillatory convection in a porous medium heated from below. *J. Fluid Mech.* **66**, 339–352.

HORNE, R. N. & O'SULLIVAN, M. J. 1978 Origin of oscillatory convection in a porous medium heated from below. *Phys. Fluids* **21**, 1260–1264.

HOWARD, L. N. 1964 Convection at high Rayleigh number. In *Proc. 11th Int. Congr. Appl. Mech., München* (ed. H. Görtler), pp. 1109–1115. Springer.

KOSCHMIEDER, E. L. 1966 On convection on a uniformly heated plane. *Beitr. Phys. Atmos.* **39**, 1–11.

KOSCHMIEDER, E. L. 1969 On the wavelength of convective motions. *J. Fluid Mech.* **35**, 527–530.

KOSTER, J. N. 1980 Freie Konvektion in vertikalen Spalten. Dissertation, Universität Karlsruhe. *KfK-Rep.* nr. 3066.

KOSTER, J. N. 1982 Heat transfer in vertical gaps. *Int. J. Heat Mass Transfer* **25**, 426–428.

KRISHNAMURTI, R. 1973 Some further studies on the transition to turbulent convection. *J. Fluid Mech.* **60**, 285–303.

KVERNVOLD, O. 1979 On the stability of non-linear convection in a Hele-Shaw cell. *Int. J. Heat Mass Transfer* **22**, 395–400.

LAMB, H. 1975 *Hydrodynamics*, 6th edn. Dover.

LAPWOOD, E. R. 1948 *Convection of a fluid in a porous medium. Proc. Camb. Phil Soc.* **44**, 508–521.

MAURER, J. & LIBCHABER. 1979 Rayleigh–Bénard experiment in liquid helium; frequency locking and the onset of turbulence. *J. Phys. (Paris) Lett.* **40**, 419–423.

SPARROW, E. M., GOLDSTEIN, R. J. & JONSSON, V. K. 1964 Thermal instabilities in a horizontal fluid layer: effect of boundary conditions and non-linear temperature profile. *J. Fluid Mech.* **18**, 513–528.

STORK, K. & MÜLLER, U. 1972 Convection in boxes: experiments. *J. Fluid Mech.* **54**, 599–611.

WILLIS, G. E., DEARDORFF, J. W. & SOMERVILLE, R. C. J. 1972 Roll-diameter dependence in Rayleigh convection and its effect upon the heat flux. *J. Fluid Mech.* **54**, 351–367.

WOODING, R. A. 1960 Instabilities of a viscous liquid of variable density in a vertical Hele-Shaw cell. *J. Fluid Mech.* **7**, 501–515.